Early Results from Chandra observations of Supernova Remnants

David N. Burrows[a], Eli Michael[b], Una Hwang[c], Roger Chevalier[d],
Gordon P. Garmire[a], Jeff Hester[e], Stephen S. Holt[c], John P. Hughes[f], Karen Lewis[a],
Richard McCray[b], John A. Nousek[a], Rob Petre[c] Patrick Slane[g] Leisa Townsley[a]

[a] Dept. of Astronomy & Astrophysics, Penn State Univ., University Park, PA 16802
[b] JILA, University of Colorado
[c] NASA/Goddard Space Flight Center
[d] University of Virginia
[e] Arizona State University
[f] Rutgers University
[g] Smithsonian Astrophysical Observatory

ABSTRACT

We present preliminary results from observations of supernova remnants by the *Chandra* X-ray Observatory (CXO). The data include imaging spectroscopy from objects observed with both GTO and GO data. The high spatial resolution of *Chandra* is revealing a wealth of small-scale structure in these remnants. Specifically, we have resolved the remnant of SN1987A, have discovered fine-scale structure in N103B and G292+1.8, and are following the temporal evolution of fine-scale structure in the Crab nebula.

1. INTRODUCTION

The *Chandra* X-ray Observatory (CXO), launched on July 23, 1999, brings unprecedented angular resolution to the field of X-ray astronomy. The CXO has two focal plane instruments, the High Resolution Camera and the Advanced CCD Imaging Spectrometer (ACIS), and two sets of transmission gratings that can be inserted into the light path to produce dispersed spectra. The subarcsecond resolution of *Chandra* finally places X-ray astronomy on par with optical ground-based astronomy in terms of imaging resolution.

The ACIS instrument team has pursued a GTO program which concentrates on observations of a wide variety of objects that utilize the high resolution imaging spectroscopy capabilities of the *Chandra*/ACIS combination. Here we present preliminary results from the first set of our GTO observations of supernova remnants, concentrating on SN1987A, for which we have the most complete analysis at this time. These data highlight the impressive capabilities of this unique observatory.

2. DATA ANALYSIS

2.1. SN1987A

Supernova 1987A (SN1987A) is particularly important because it provides a unique opportunity for detailed study of the earliest stages of a supernova remnant, in an object at a known distance (50 kpc) and with a known progenitor (Sanduleak -69 202, a B3 I blue supergiant). It was the first supernova in nearly 400 years that was bright enough to be visible to the naked eye, and was the brightest supernova (SN) in the era of modern astronomical (including space-based) instruments. As a result, it has been studied across the entire electromagnetic spectrum, and is the only SN explosion from which a neutrino burst has been detected[2], confirming our theoretical models of stellar collapse.

The structure of SN1987A has been mostly clearly seen in HST observations such as that shown in Figure 1. The HST image shows a bright elliptical ring (1.7×1.2 arcseconds) surrounding the optical remnant. Surrounding the inner ring are two fainter outer rings. We focus here on the inner ring, which has been interpreted as a ring of high-density material in the equatorial plane, caused by the impact of the high velocity stellar wind of the blue giant progenitor with its earlier, slower red giant wind, and ionized by the UV flash from the supernova explosion 13 years ago[5].

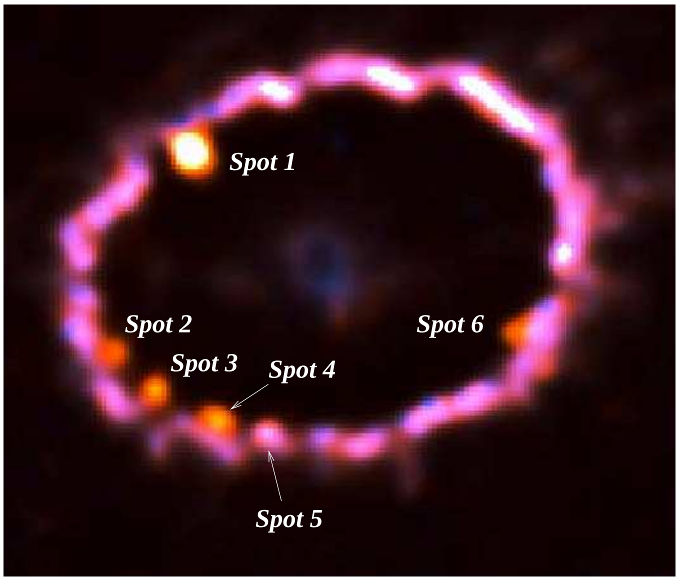

Figure 1. HST Hα image of SN1987A taken on 2 February 2000, courtesy of P. Challis, R. Kirshner, and P. Garnavich. The optical hot spots are labeled using the nomenclature of Garnavich, Kirshner, and Challis[12]. This image is rotated counter-clockwise by 25° with respect to the other images in this paper.

In recent years, HST observations of SN1987A have revealed a gradually brightening optical "hot spot" on the inner ring at a position angle of 29 degrees[6] (Spot 1). This hot spot has been interpreted as a protrusion of gas from the inner ring back towards the central object, which is being heated as the supernova shock front has begun engulfing it[7]. When the shock front hits the remainder of the inner ring, the remnant is expected to brighten by as much as three orders of magnitude at optical, UV, and X-ray wavelengths[8]. In the past several months, HST observations have shown that at least four new optical hot spots have begun to glow along the eastern inner edge of the inner ring[9−12], providing further evidence that the shock front is beginning to interact with the circumstellar nebula.

At radio wavelengths, ATCA observations have shown a steadily expanding and brightening shell-like remnant[13,14]. An image made on 9 September 1999 is shown in Figure 2b. The remnant has a two-lobed structure peaking just inside the optical inner ring, with the eastern lobe about twice as bright as the western lobe. The radio emission fills the inner optical ring.

We have observed SN1987A twice with the *Chandra X-ray Observatory*[16] as part of the *Chandra* GTO program. The *Chandra* mirrors have angular resolution of 0.5 arcseconds HPD on-axis. There are two focal plane cameras and two sets of transmission gratings that can be inserted into the optical path. Our observations utilized the Advanced CCD Imaging Spectrometer (ACIS)[17], which takes high resolution images with moderate non-dispersive energy resolution, and which can also serve as a readout device for the transmission gratings. Our first observation was made on 6 October 1999 using the High Energy Transmission Grating and the ACIS-S detector array. This 120 ks observation produced an undispersed zero-order image of the remnant with moderate energy resolution, and a set of dispersed spectra with high energy resolution. The second observation, made on 17 January 2000, used the ACIS S3 detector and provided 10.7 ks of data with moderate nondispersive energy resolution.

The data were processed and filtered to reduce the background. We restricted photon energies to 0.3–8 keV and used ASCA grade 02346 events. In order to obtain the highest possible spatial resolution, we turned off the pixel randomization introduced by the standard data processing sytem. The lightcurves were examined for times of high background that could contaminate our results, but none were found. The first observation contained 696 photons meeting our criteria, while the second observation had 583 photons. Other than the data screening/processing discussed above, no background subtraction was required for this analysis, because the background rate is negligible over the area covered by a near-pointlike object at the telescope focus. The astrometry of the raw images was adjusted by hand to agree with the reference system of Reynolds *et al.*[18], who determined a position of (05:35:27.97,

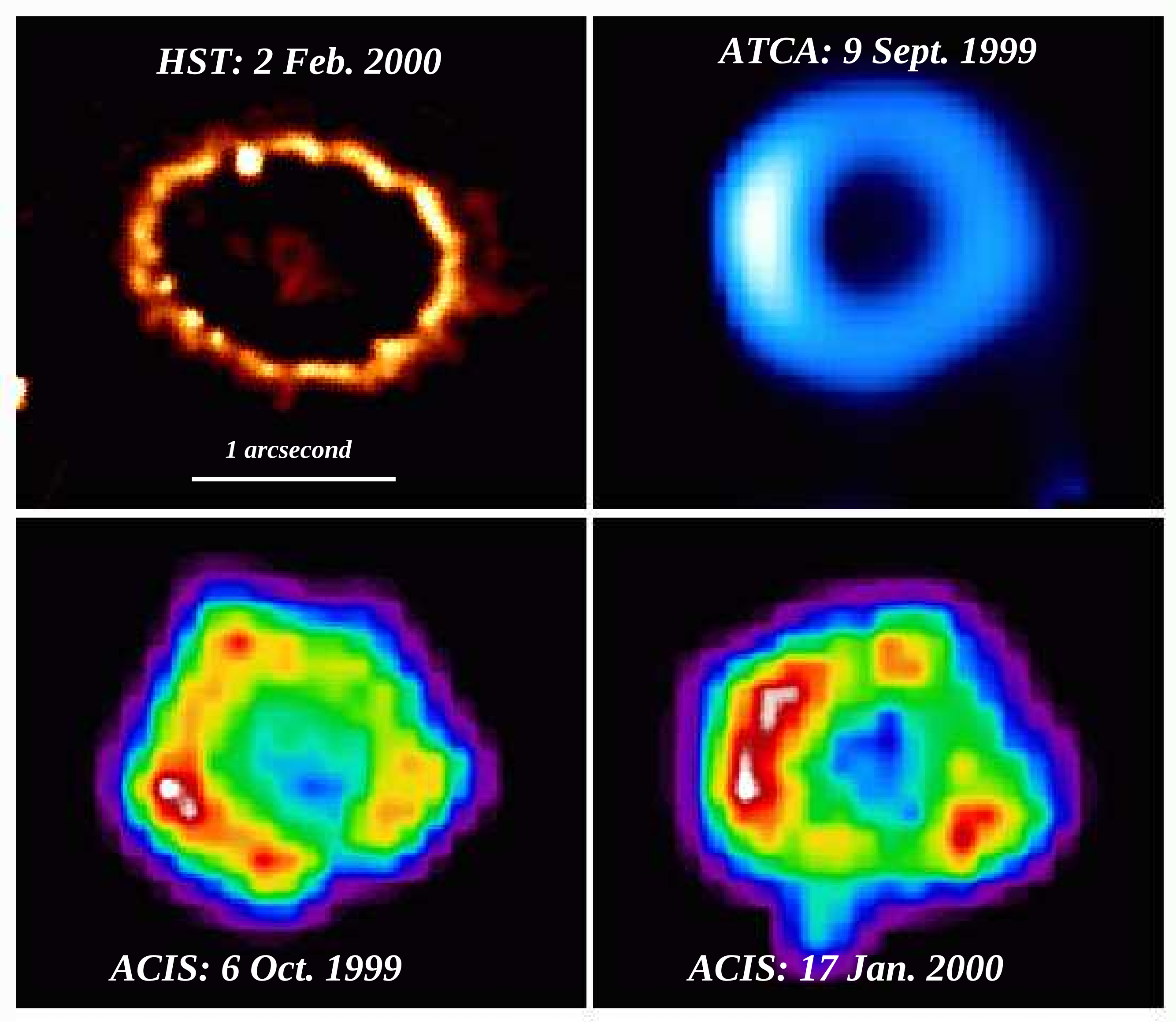

Figure 2. Four recent images of SN1987A: a: HST image (Garnavich, Kirshner, and Challis[12]) taken on 2 February 2000; b: deconvolved ATCA 8 GHz image from 9 September 1999 (Manchester *et al.*[14]); c: deconvolved ACIS image of SN1987A from 6 October ; d: deconvolved ACIS image of SN1987A from 17 January 2000. The images are made with identical scaling and orientation (north is up). The ATCA data were kindly made available to us for this comparison by Bryan Gaensler and Dick Manchester. The Australian Telescope Compact Array is funded by the Commonwealth of Australia for operation as a National Facility managed by CSIRO.

-69:16:11.09) for SN1987A based on Hipparcos and VLBI data, and to permit alignment of the X-ray, optical, and radio images to subarsecond accuracy.

The optical and radio remnants measure roughly $1.7'' \times 1.2''$ g on the sky, as do the raw X-ray images. This is barely resolved by the *Chandra*/ACIS instrument, which has $\sim 0.5''$ imaging from the telescope and $0.492''$ pixels in the detector. Because *Chandra* moves slowly across the sky during each observation, the placement of ACIS detector pixels on the sky is not fixed during an observation, allowing us to deconvolve the images to an effective resolution greater than the telescope resolution. The ACIS data were binned into 0.125 arcsecond sky pixels, and the resulting images were then deconvolved with a Maximum Likelihood algorithm (20 iterations), using an on-axis point spread function obtained with the MARX ray tracing software package. Smoothed versions of the deconvolved images are shown in Figure 2c and 2d, and have an effective resolution of about 0.3 arcseconds (FWHM). Monte Carlo simulations show that the bright features in these images are significant; this is confirmed by the fact that most of them are present in both the October 1999 and the January 2000 deconvolved images (Figure 2c and 2d).

The SNR is shell-like, with the X-ray emission peaking just inside the optical inner ring, as expected on the basis of current models[19,7]. The X-ray remnant size, measured between peaks of the shell, is 1.17×0.98 arcseconds. The brightest X-ray emission does *not* coincide with the bright optical "hot spot" (Spot 1) at position angle 30° in the northeast quadrant; instead, the X-ray emission peaks along the eastern edge of the remnant, close to the newly discovered optical hot spots that have just become visible in the past several months. UV observations made with HST show very strong Lyα and Hα emission from the eastern quadrant where the new hot spots are appearing. We believe that the X-ray emission in this region is produced by debris crossing the reverse shock, which has a velocity of about 15,000 km/s. The hot ejecta trapped between the reverse shock and the forward blast wave is acting as a piston to push the blast wave forward into the ring in this region, producing new optical hot spots as the blast wave begins to engulf material from the inner ring.

Figure 3 shows the two X-ray images, overlaid with plots of the HST Hα contours. The position angles of both

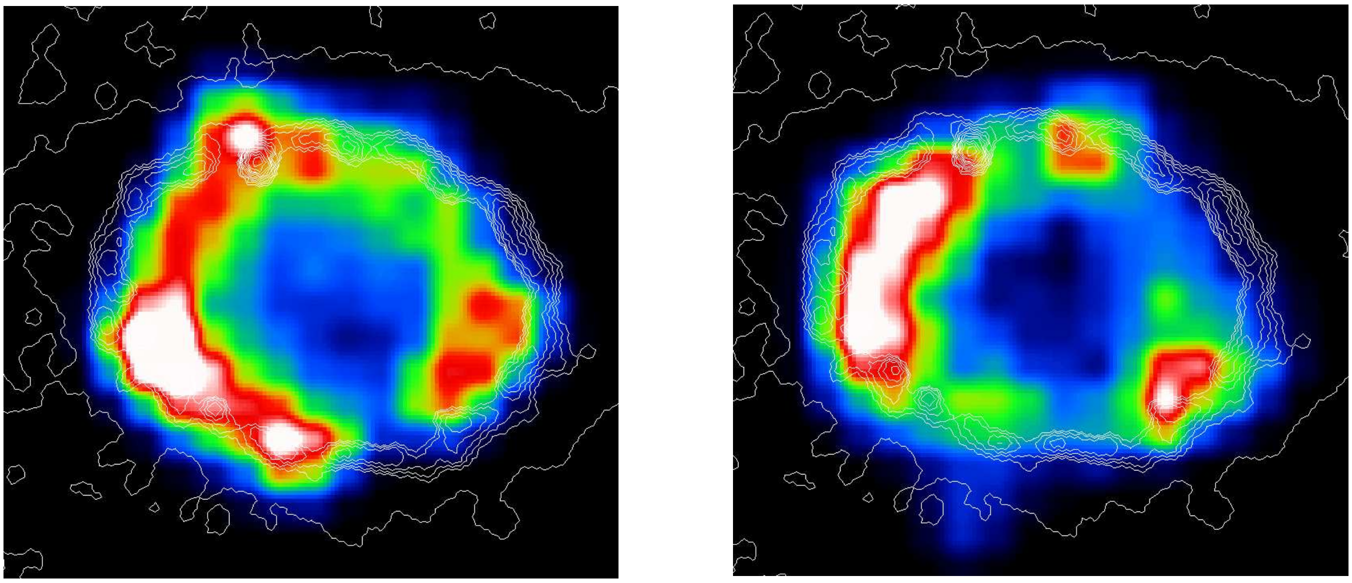

Figure 3. ACIS deconvolved images of SN1987A, with the Feb. 2000 HST image overlaid as contours. a: 6 Oct 1999 observation. b: 17 Jan 2000 observation.

the optical hot spots and X-ray peaks are given in Table 1. Some of the X-ray peaks agree extremely well with optical

Table 1. Position angles of hot spots

Optical Hot Spots:	Spot 1		Spot 2	Spot 3	Spot 4	Spot 5		Spot 6	
X-ray Peaks:	A	B	C	D		E	F	G	H
HST†: Feb. 2000	29°		91°	106°	122°	139°		229°	
ACIS: Oct. 1999	32°		98°	108°			156°	240° – 270°	
ACIS: Jan. 2000		65°		103°			155°	230°	345°

hot spot positions (e.g., Spot 1/A; Spot 2/C; Spot 3/D; and Spot 6/F). (The small misalignment between Spot 1 and Peak A in Figure 3a is not signicant.) In other regions, we see X-ray peaks without corresponding optical hot spots (e.g., B, F, and H), or optical hot spots without corresponding X-ray peaks (Spots 4, 5). We note that our second observation has no X-ray peak corresponding to Spot 1. This may be due to different spectral responses between the two observations (taken with and without the grating inserted into the beam); it may reflect a temporal variation in the X-ray structure; or it may be due to counting statistics. Longer observations are required to elucidate this; we plan to make such an observation during Cycle 2.

We see no evidence for a point source in the interior of SN1987A. However, this may be due to the fact that we are barely resolving the remnant; a point source would be difficult to find at this resolution. We have performed a Monte Carlo simulation to determine our point source sensitivity. In this simulation, we add a point source of various intensities to the observed photon image, then perform the deconvolution. This allows us to place an upper limit of 10% on the contribution of a central point source to this object. The central source luminosity is less than 10^{34} ergs/s.

We have performed spectral fits using the 0^{th} order image from our 1999 observation. We used a detailed Monte Carlo model of the X-ray interaction processes within the CCD detector to correct the photon events for charge trailing and charge loss produced by imperfect Charge Transfer Efficiency (CTE)[20]. We used spectral response matrices

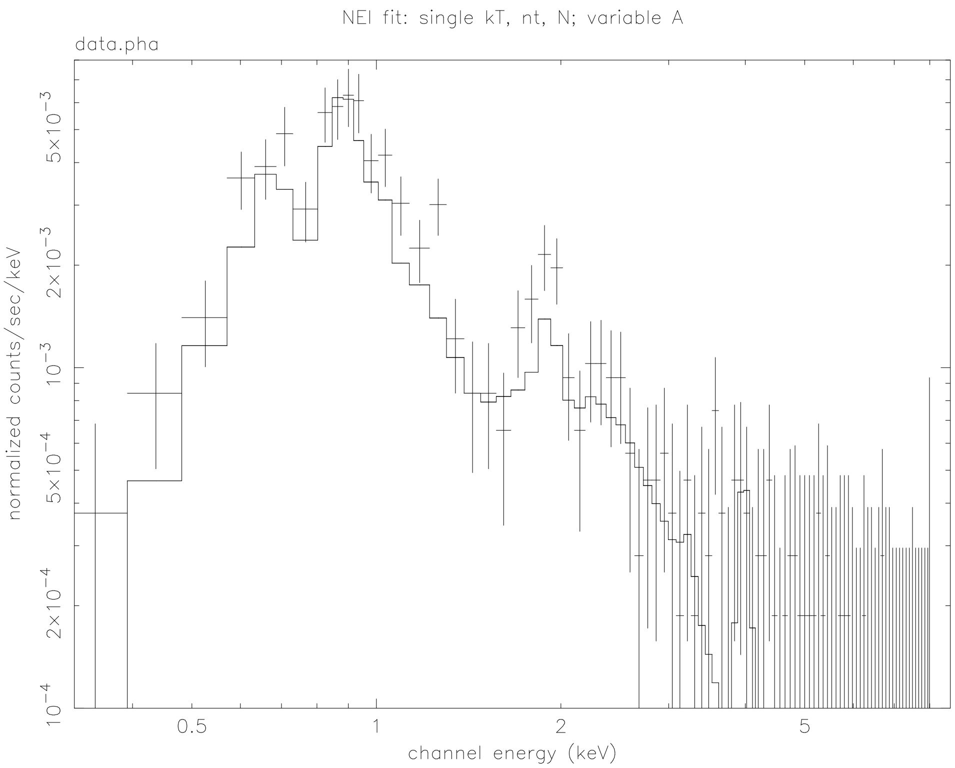

Figure 4. Best fit of a nonequilibrium ionization plasma model with solar abundances to the zero-order spectrum.

appropriate for an on-axis source on the S3 detector, with a gain correction (4%, emperically determined) to adjust for the fact that our photon event amplitudes have been corrected for CTE. The spectrum cannot be fitted with any simple continuum model or with any solar abundance collisional ionization equilibrium plasma model. Acceptable fits require either increased abundances of C- and Si-burning products or nonequilibrium ionization (Table 2). A sample spectral fit is shown in Figure 4. The spectrum can be fitted well with either variable abundance collisional ionization equilibrium models with enhanced C- and Si-burning products, or with nonequilibrium ionization models closer to solar abundances, but still significantly enhanced with respect to LMC abundances.

Our first observation produced a dispersed high resolution spectrum in addition to the 0^{th} order image discussed above. A preliminary reduction of the dispersed spectrum is shown in Figure 5. The Chandra High Energy Transmission Grating consists of two types of grating elements, which are optimized for medium and high energies. The MEG and HET elements are installed at slightly different angles so that the dispersed spectra form a shallow X on the readout array. The dispersed data were processed with the gain tables appropriate for the degraded on-orbit response of the front-illuminated CCDs. Photons with the correct energy for their position along the dispersed

Table 2. Nondispersive spectral fit results

Model	N_H (10^{22} cm^{-2})	kT (keV)	α	χ^2	Notes
Power Law:	0.34		3.2	376	
Bremsstrahlung:	0.19	1.1		381	
Plasma (Raymond-Smith):	0.05	1.0		394	
Variable Abundances:					
Raymond-Smith:	0.67	0.67		299	N, O, Si, S high
RS + Power Law:	0.16	0.68	0.10	288	C, N, O, Si high
Nonequilibrium Ionization:			nt		
Solar Abundances:	0.57	2.36	10.5	288	
Variable Abundances:	0.60	2.20	10.5	288	C, O high

spectrum were extracted for further processing, using a 3 arcsecond wide extraction region to optimize the signal to noise ratio. Background subtraction was performed using background regions 7.5 seconds wide located on either side of the source spectrum. Photons from the positive and negative order of both gratings were co-added to produce the spectrum shown in Figure 5. The spectrum is dominated by bright lines from the Helium-like and Hydrogen-like

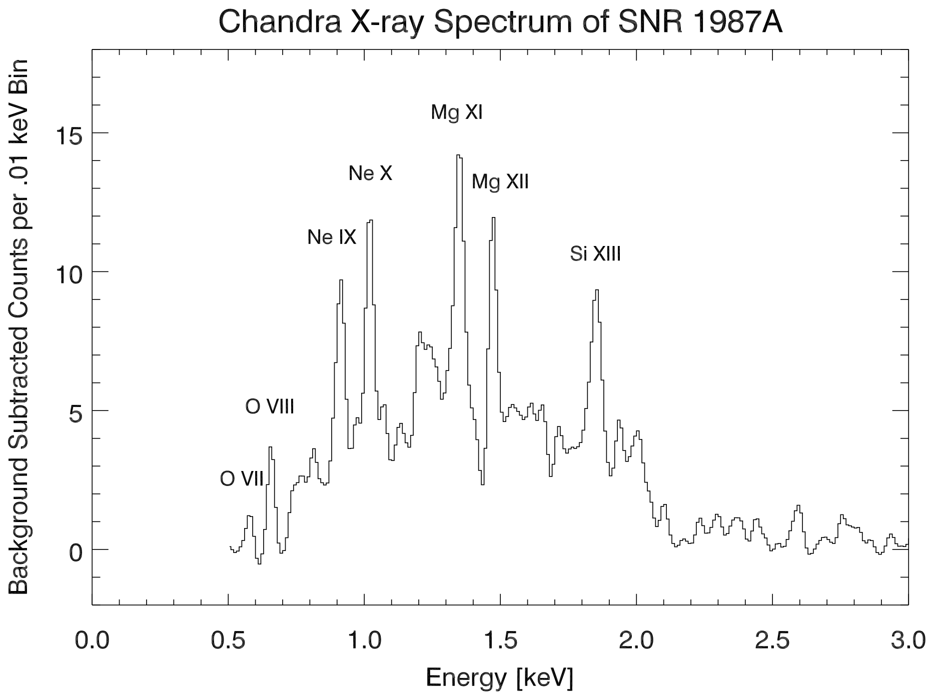

Figure 5. Dispersed X-ray spectrum of SN1987A.

ionization stages of O, Ne, Mg, and Si, confirming the conclusions derived from the non-dispersed spectrum.

If the line shapes are dominated by Doppler shifts from the bulk motion of the rapidly expanding young remnant, then it is possible to determine the geometry of the remnant from the X-ray line profiles, given sufficiently high energy resolution. We have co-added four of the brightest X-ray lines and smoothed the resulting profile with a 1000 km/s Gaussian to produce the average line profile shown in Figure 6. This composite line profile has a nearly Gaussian shape with full width at base of 8000 km/s, consistent with a blast wave speed of about 4500 km/s.

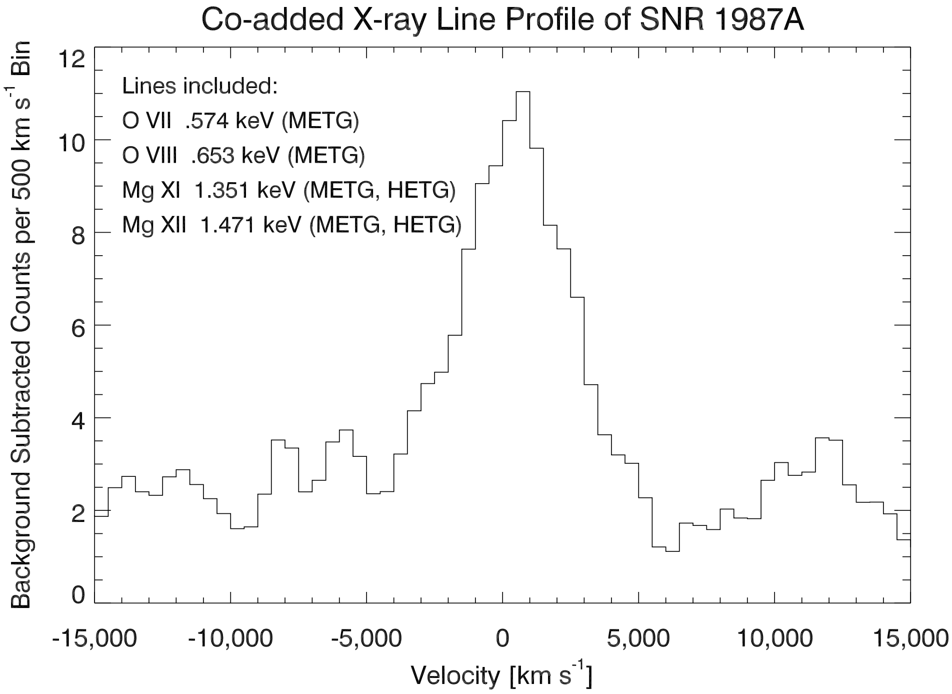

Figure 6. Co-added spectral line profile.

2.2. Cas A

The first light target of *Chandra* was the Cas A supernova remnant. These data were made public as part of the calibration database, and we have performed preliminary analysis of them. A "true color" image of Cas A is shown in Figure 7. There are both spatial and spectral variations on all size scales down to the resolution limit of the *Chandra* telescope. We have found clear evidence for turbulent expansion of the SN ejecta, with Fe-rich material from the innermost portions of the progenitor clearly outside Si-rich material produced by explosive oxygen burning in overlying layers. However, the ejecta are not mixed on a fine scale, and contain many filaments that appear to be dominated by material from a single shell. For further details, please see Hughes *et al.*[21]

2.3. G292+1.8

G292 is one of a small class of oxygen-rich supernova remnants, which includes Cas A and N132D in the LMC. Radio observations of the remnant give a spectral index between that typical for shell-like remnants and plerions. X-ray spectral observations show indications of nonthermal emission from the central region, suggesting that G292 may be a composite remnant: a thermal remnant with a plerionic core.

We observed G292 with the S3 detector of the *Chandra* ACIS instrument for 43.2 ks on 11 March 2000, obtaining nearly 3 million counts. A broadband image of G292 is shown in Figure 8, and a preliminary spectrum of the entire remnant is shown in Figure 9. The remnant is similar to Cas A in terms of the tremendous amount of small-scale spatial detail. The full data will allow us to perform detailed spectroscopy of individual filaments and to investigate the central jet-like structure.

2.4. N103B

N103B is a bright remnant in the LMC. Our 40.8 ks *Chandra* observation was obtained on 4 December 1999, and contains 280,000 counts. An adaptively smoothed broad band image is shown in Figure 10. The remnant is about 20 arcseconds in diameter, with spatial structure on subarcsecond scales clearly visible. The eastern rim of the remnant appears to exhibit Rayleigh-Taylor instabilities; these are not apparent on the western rim.

The spectrum of the entire remnant is shown in Figure 11. The spectrum is dominated by lines of Si, S, Ar, Ca, and Fe. There is no evidence of O lines in the spectrum.

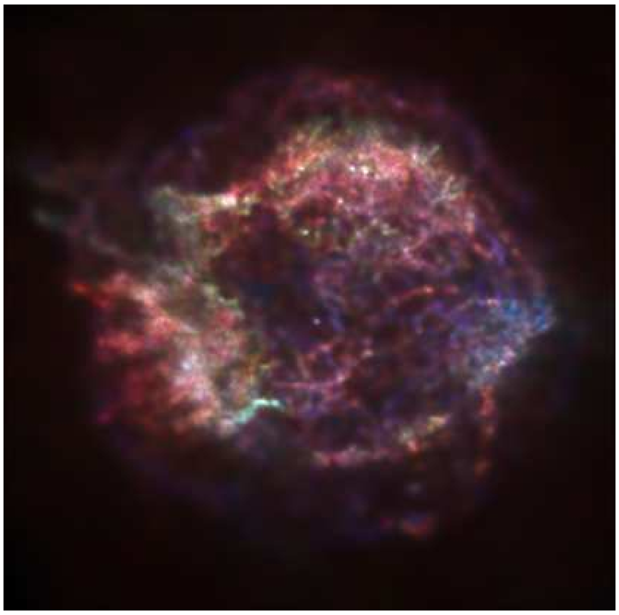

Figure 7. True X-ray colors of Cas A. Red colors indicate emission between 0.6 and 1.65 keV (dominated by Fe-L lines), green indicates emission between 1.65 and 2.25 keV (dominated by Si K lines), and blue indicates emission dominated by photons above 2.25 keV. From Hughes *et al.*[21].

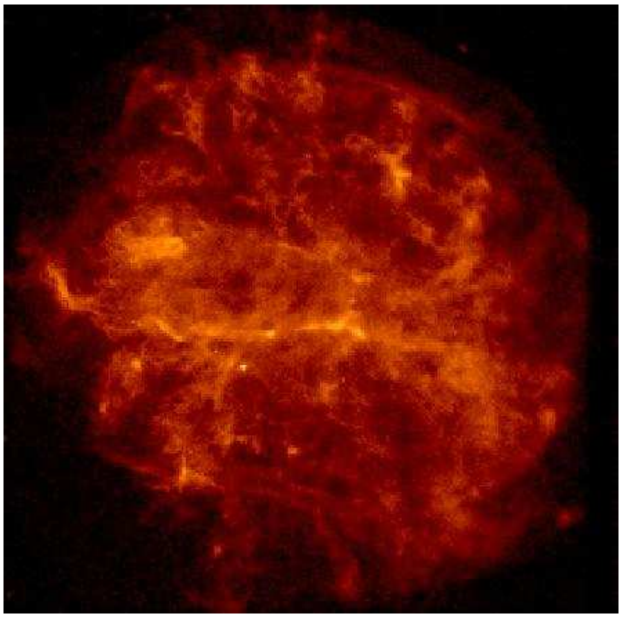

Figure 8. Preliminary broad-band image of G292+1.8.

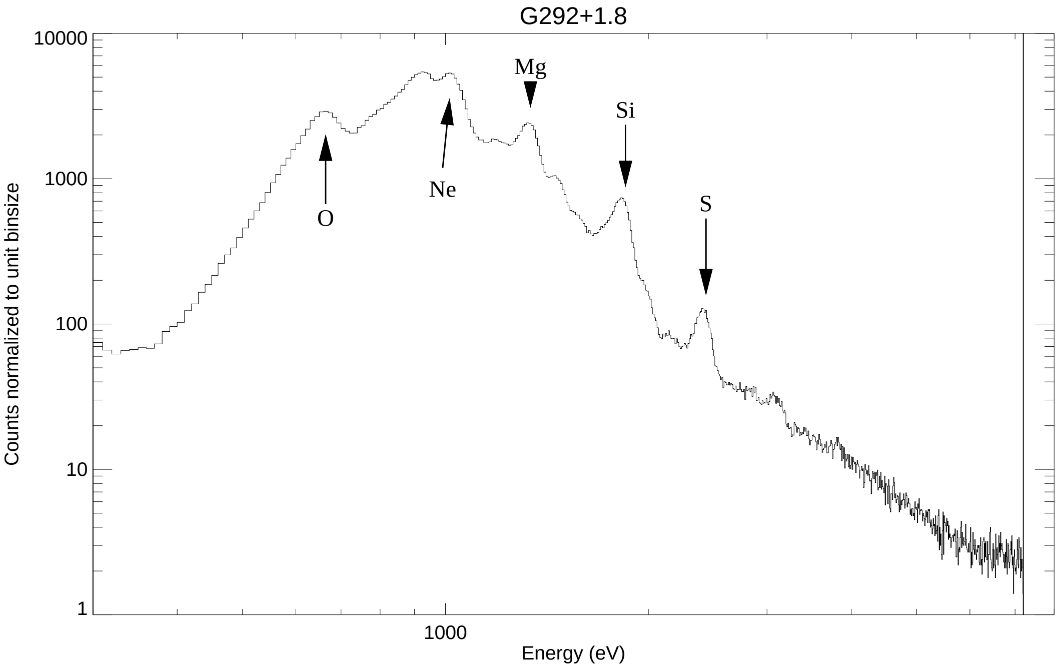

Figure 9. Preliminary spectrum of G292+1.8.

In order to investigate the spatial distribution of the ejecta, we have made images of the remnant in the energies of individual bright lines, and have computed ratios of these line images. As an example, we show an image of the Si/S ratio in Figure 12. The line ratio varies from a low of 2.0 to a high of 5.0 across the remnant. Some of the

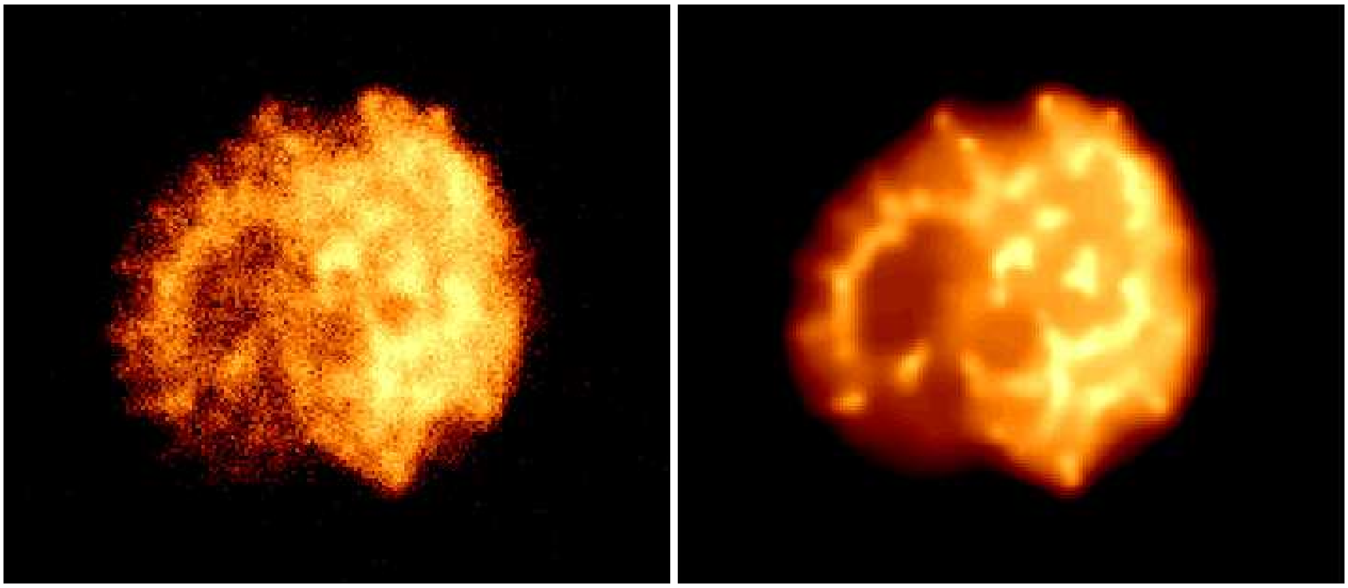

Figure 10. Broadband image of N103B in the LMC. a) Raw image. b) Adaptively smoothed image.

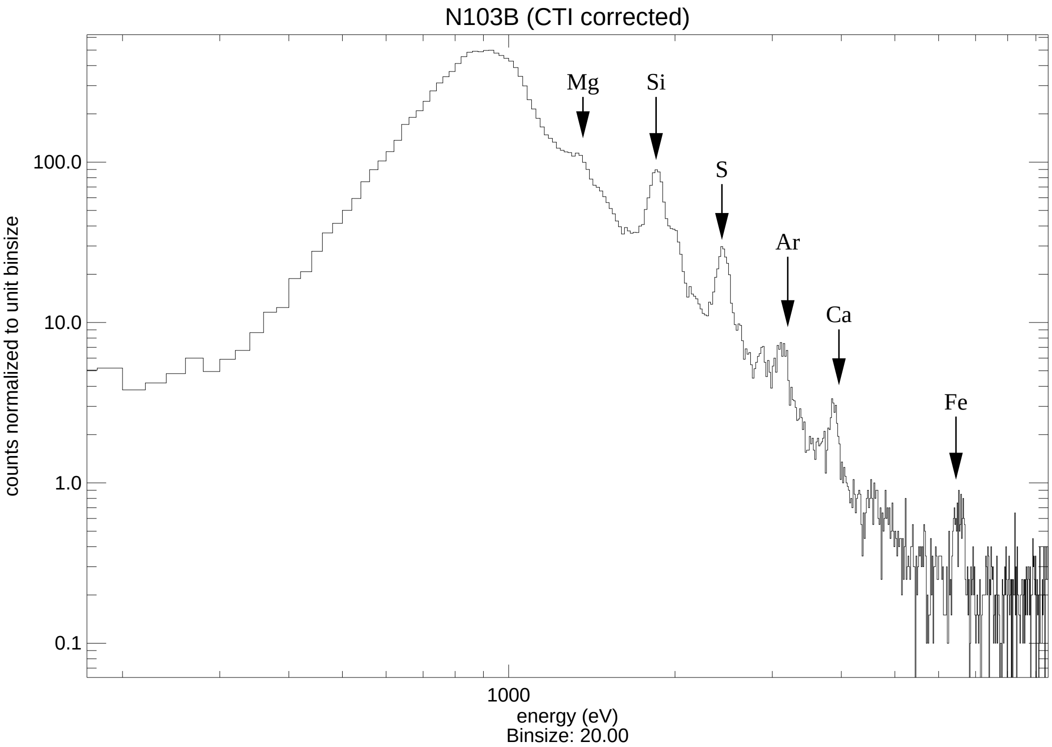

Figure 11. Chandra spectrum of N103B in the LMC.

features in the line ratio image trace features in the broad-band image, but others do not. Additional analysis will be required to unravel the combined spatial and spectral variations that we observe.

3. CONCLUSIONS

The *Chandra X-ray Observatory* has opened up an exciting new era of high spatial and spectral resolution X-ray astronomy, which is making it possible for us to follow the development of this very young supernova remnant (SNR),

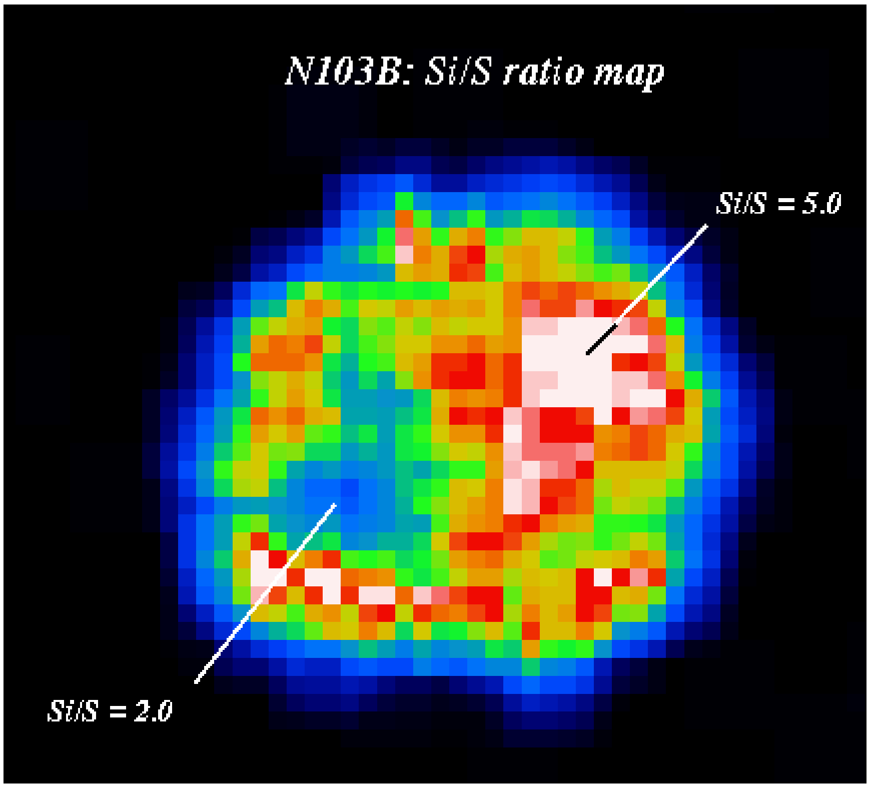

Figure 12. Ratio of Si/S. The lowest value is about 2.0, and the highest value is about 5.0.

and to confront theoretical models of SNR evolution with detailed X-ray observations for the first time. The results discussed here provide a glimpse of the qualitatively new results that will be produced by detailed analysis of these data in the coming years.

ACKNOWLEDGEMENTS

This work was supported by NASA contract NAS8-38252. We are grateful to Bryan Gaensler and Peter Challis for providing their data for comparison with our *Chandra* observations.

REFERENCES

1. P. Andreani, R. Ferlet, and A. Vidal-Madjar, *Nature*, **326**, 770 (1987).
2. M. Koshiba, *et al.*, *IAU Circ.*, **4338** (1987).
3. R. P. Kirshner, *et al.*, *Astrophys. J.*, **320**, 602 (1987).
4. G. Sonneborn, B. Altner, and R. P. Kirshner, *Astrophys. J.*, **323**, L35 (1987).
5. C. J. Burrows, *et al.*, *Astrophys. J.*, **452**, 680 (1995).
6. P. Garnavich, *et al.*, *Astrophys. J.*, **TBD**, TBD, (1999).
7. E. Michael, *et al.*, *Astrophys. J.*, **TBD**, TBD, (2000).
8. D. Luo, R. McCray, & J. Slavin, *Astrophys. J.*, **430**, 264 (1994).
9. P. Bouchet, *et al.*, *IAU Circ.*, **7354** (2000).
10. S. Lawrence and A. Crotts, *IAU Circ.*, **7359** (2000).

11. S. Maran, C. S. J. Pun, and G. Sonneborn, *IAU Circ.*, **7359** (2000).

12. P. Garnavich, R. Kirshner, and P. Challis, *IAU Circ.*, **7360** (2000).

13. B. Gaensler *et al.*, *Astrophys. J.*, **479**, 845 (1997).

14. R. Manchester, *et al.*, PASA, in prep (2000)

15. G. Hasinger, B. Aschenbach, and J. Trümper, *Astron. Astrophys.*, **312**, L9 (1996).

16. TBD

17. TBD

18. J. E. Reynolds, *et al.*, *Astron. Astrophys.*, **304**, 116 (1995).

19. R. A. Chevalier and V. V. Dwarkadas, *Astrophys. J.*, **452**, L45 (1995)

20. L. Townsley, /etal, in prep (2000).

21. J. Hughes, C. Rakowski, D. N. Burrows, and P. Slane, *Astrophys. J.*, **TBD**, TBD (2000).